Paul H. Mayrhofer[a,b,c], Lars Hultman[c], Jochen M. Schneider[a], Peter Staron[d], Helmut Clemens[b]

[a] Materials Chemistry, RWTH-Aachen, Aachen, Germany
[b] Department of Physical Metallurgy and Materials Testing, Montanuniversität Leoben, Leoben, Austria
[c] Thin Film Division, Department of Physics (IFM), Linköping University, Linköping, Sweden
[d] Institute for Materials Research, GKSS Research Centre, Geesthacht, Germany

Spinodal decomposition of cubic $Ti_{1-x}Al_xN$: Comparison between experiments and modeling

Dedicated to Professor Dr. Hellmut Fischmeister on the occasion of his 80th birthday

Annealing of cubic (c) $Ti_{1-x}Al_xN$, possessing NaCl structure, leads to decomposition into the stable constituents c-TiN and hexagonal (h) AlN (ZnS wurtzite structure) via the formation of metastable c-TiN rich and metastable c-AlN rich phases. In this paper, we describe the influence of sizes of the newly formed particles and strain energy due to their different lattice parameter and elastic constants with respect to the remaining matrix on decomposition processes and energetics. Good agreement between the enthalpy output obtained from differential scanning calorimetry and values derived from ab-initio and continuum mechanical based calculations for the decomposition and transformation processes occurring is obtained. Based on the comparison between experiments including X-ray diffraction and small-angle neutron scattering of annealed samples and modeling we can conclude that spinodal decomposition is present in c-$Ti_{1-x}Al_xN$ coatings with $x = 0.50$ and 0.66, whereas the alloy with $x = 0.25$ is outside the spinodal.

Keywords: Ab-initio calculation; Calorimetry; Small-angle neutron scattering; Decomposition; TiAlN

1. Introduction

Cubic (c) $Ti_{1-x}Al_xN$, possessing NaCl structure, has valued properties for many different industrial applications such as wear protection of tools, dies, molds, as a corrosion-resistant coating on mechanical components [1, 2] as well as a diffusion-barrier in microelectronic devices [3]. Spinodal decomposition in ceramic materials in general and thin films in particular is a relatively unexplored field, although it effectively influences the materials properties [4–6]. The term 'spinodal' depicts the boundaries between metastable and unstable regions of the phase diagram where the diffusion coefficient is negative [7]. These boundaries were first described by a thermodynamic concept as the limit of metastability for fluid phases by Gibbs in 1877 [8]. The difficulties in preparing actually unstable ceramic materials deep within the spinodal region can be overcome by implementing plasma assisted vapor deposition techniques with their capacity for extremely high cooling rates ($\sim 10^{13}$ K s^{-1}, see Ref. [9]). Cahn mentions in his work that the requirement for the spinodal process in a solid is the continuous formation process of the new phases. This severely limits the kinds of solid phases that can form to ones crystallographically similar to the original phase [10]. Due to their similar crystallography and the fact that nm-sized phases are of particular interest in designing materials properties, experimental observation of spinodal decomposition by transmission electron microscopy is challenging.

Ab-initio calculations show that the lattice parameter (a) of supersaturated cubic $Ti_{1-x}Al_xN$ continuously decreases from 4.255 Å for c-TiN to 4.069 Å for c-AlN with increasing AlN mole fraction x [11]. Thus, the maximum deviation in calculated lattice parameters is $\sim 4.5\,\%$. Annealing of c-$Ti_{1-x}Al_xN$ leads to phase transformation into the stable phases c-TiN and hexagonal (h) AlN (wurtzite structure) via the formation of metastable cubic TiN rich and metastable cubic AlN rich phases, respectively, implementing the spinodal decomposition mechanism [4]. The h-AlN in turn forms by nucleation and growth from the cubic AlN or TiN depleted $Ti_{1-x}Al_xN$ alloy. Recently, we have reported that the chemical requirements for spinodal decomposition are fulfilled for supersaturated c-$Ti_{1-x}Al_xN$ over a wide temperature and composition range [12]. Furthermore, we have described the contribution of strain and surface energy on the energetic balance for this decomposition process [13]. However, a detailed comparison between modeled and experimentally obtained results for the decomposition process of c-$Ti_{1-x}Al_xN$ is still missing.

In this study, we discuss results obtained by differential scanning calorimetry (DSC), X-ray diffraction (XRD) as well as small-angle neutron scattering (SANS) with respect to ab-initio and continuum mechanical approaches. Based on this combination, the spinodal contribution to the decomposition of supersaturated cubic $Ti_{1-x}Al_xN$ coatings and the contributions of strain and grain size are investigated.

2. Experimental and modeling procedures

$Ti_{1-x}Al_xN$ films, $\sim 3\mu$m thick, are grown on polished low-alloy steel substrates at 500 °C by a commercial arc evaporation system (Metaplas MR323) from Ti, $Ti_{0.75}Al_{0.25}$, $Ti_{0.5}Al_{0.5}$, and $Ti_{0.33}Al_{0.67}$ targets (63 mm in diameter) in N_2 (99.995 % purity) atmosphere. The deposition system and growth conditions are described in more detail in Ref. [14], chemical analyses are described in Ref. [15]. For all

experimental investigations the low-alloy steel substrates of the as-deposited $Ti_{1-x}Al_xN$ films are dissolved in 10 mol.% nitric acid in order to eliminate possible interference with the substrate. Structure and phase composition of the films are determined by Bragg–Brentano X-ray diffraction with Cu-K_α radiation using a Siemens D 500 diffractometer.

Phase and structural changes in the $Ti_{1-x}Al_xN$ films are followed as a function of post-deposition annealing temperature using a Netzsch-STA 409 differential scanning calorimeter. The atmospheric pressure DSC experiments are carried out in flowing Ar (99.999 % purity and 50 sccm) to minimize sample oxidation. Statistical investigations of the DSC measurements, which were repeated five times for samples with $x = 0.50$ and 0.66, indicate a maximum error for the enthalpy values of 10 %. Subsequent to DSC measurements, where bidirectional temperature excursions from room temperature (RT) to individual temperatures to RT at heating and cooling rates of 50 K min^{-1} are conducted, the samples are again analyzed by XRD. The maximum investigation temperature is 1400 °C.

Small-angle neutron scattering measurements are carried out on c-$Ti_{0.5}Al_{0.5}N$ in the as-deposited state and after DSC to 860 and 1100 °C with the instrument SANS-2 at the Geesthacht Neutron Facility (GeNF). Selector-monochromated neutrons with a mean wavelength of $\lambda = 0.57$ nm and a wavelength spread of $\Delta\lambda/\lambda = 10$ % are used. A lateral area detector is employed, which can be rotated around the sample to cover large scattering vectors q ($q = 4\pi \sin\theta/\lambda$ where 2θ is the scattering angle). Measured intensities are corrected for sample transmission, background intensity, and detector response. Macroscopic differential scattering cross-sections are obtained by calibration against the incoherent scattering of vanadium.

Ab-initio calculations of $Ti_{1-x}Al_xN$ are based on the density-functional theory using the VASP code [16], in conjunction with the generalized-gradient approximations projector augmented wave potentials [17]. Details of the calculations and the continuum mechanical approaches can be found in Refs. [11] and [13].

3. Results and discussion

XRD analyses of as-deposited coatings with $x = 0.25$, 0.50, and 0.66, reveal a single phase with cubic structure, showing stress-free lattice parameters of 4.22, 4.19, and 4.15 Å, respectively, which are in good agreement to calculated values [9, 8]. In addition to our previous report on DSC and XRD of c-$Ti_{1-x}Al_xN$ [4], here we also present results for $x = 0.25$.

Figure 1 shows typical DSC spectra (400 to 1400 °C), baseline subtracted, from our as-deposited $Ti_{1-x}Al_xN$ coatings with $x = 0$, 0.25, 0.50, and 0.66. All spectra consist of several exothermic features (composed of multiple peaks) stemming from irreversible reactions. Cooling the sample and reheating it through the same range yields a featureless DSC scan. Thus, the second scan was used as a baseline for calculating the individual enthalpy outputs from the integrated area under the DSC spectra.

The DSC peak centered at 1328 and 1216 °C for $Ti_{1-x}Al_xN$ with $x = 0.50$ and 0.66, respectively, can be related to recrystallization (formation of new crystallites where the coating structure also changes from columnar to equiaxed) [16, 17] including transformation of c-AlN into h-AlN [4] This can be seen from the comparison between Fig. 2a and b, showing XRD scans of the DSC samples heated to temperatures before and beyond this reaction. After annealing of c-$Ti_{1-x}Al_xN$ with $x = 0.25$, 0.50, and

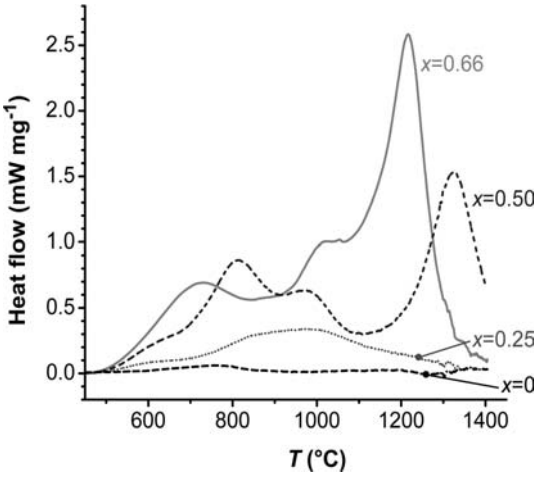

Fig. 1. Baseline subtracted DSC scans of c-$Ti_{1-x}Al_xN$ coatings with $x = 0$, 0.25, 0.50, and 0.66.

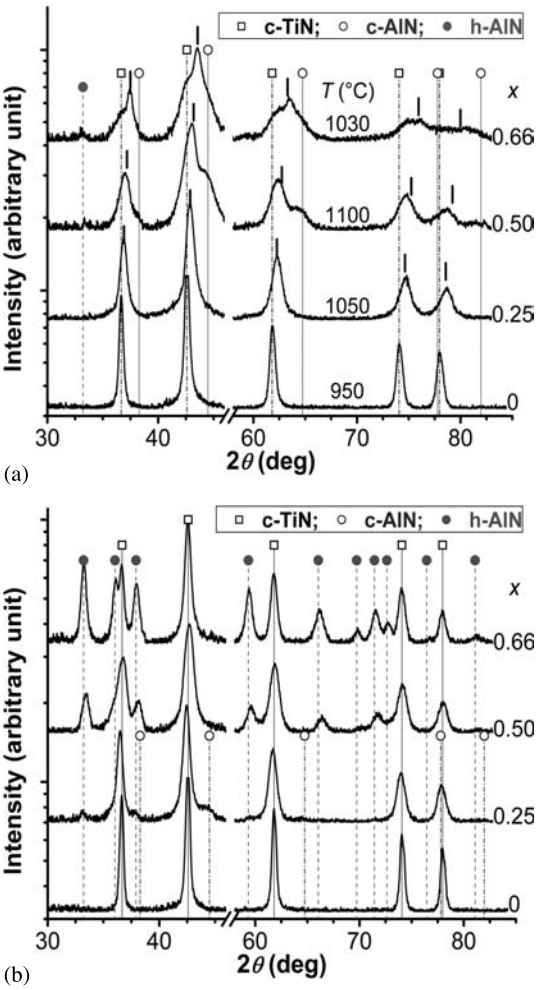

Fig. 2. Room temperature XRD scans obtained from $Ti_{1-x}Al_xN$ DSC samples with $x = 0$, 0.25, 0.50, and 0.66 after (a) heating to 950, 1050, 1100, and 1030 °C, respectively, and after (b) heating to 1400 °C. The dashes above the reflexes show the diffraction angle position calculated from lattice parameters of the respective as-deposited c-$Ti_{1-x}Al_xN$.

0.66 to $T_a = 1050$, 1100, and 1030 °C, respectively, the XRD scans (Fig. 2a) indicate the presence of c-TiN, c-AlN, and remaining matrix peaks (the dashes above the reflexes show the diffraction angle position calculated from lattice parameters of the respective as-deposited c-$Ti_{1-x}Al_xN$). A small reflex of h-AlN at 33.2° is detectable for $x = 0.66$. Further annealing of the coatings with AlN mole fractions x of 0.50 and 0.66 to 1400 °C causes a complete transformation of the spinodally formed c-AlN into h-AlN and recrystallization of the coating (Fig. 2b) [4]. The corresponding energy release (i.e., the integrated area under the DSC peaks) is 18.22 and 22.22 kJ mol^{-1} for $x = 0.50$ and 0.66, which fits the calculations of 17.54 and 23.15 kJ mol^{-1} for $x = 0.50$ and 0.66, respectively, obtained from the energy difference between c-AlN and h-AlN, which is 35.08 kJ mol^{-1} [11]. For the coating with $x = 0.25$, however, c-AlN is detected even after annealing to 1400 °C (see Fig. 2b, c-AlN reflex at 44.5°), which is the maximum temperature of the DSC unit used. Consequently, the measured enthalpy output of 3.22 kJ mol^{-1} is much smaller than the expected one of 8.77 kJ mol^{-1}, indicating that ~37 % of the formed c-AlN transformed into h-AlN.

Figure 3 shows the temperature–composition phase diagram for $Ti_{1-x}Al_xN$ with the binodals and spinodals calculated after Refs. [12] and [13]. The chemical binodal for separation into c-TiN and metastable c-AlN (indicated by c–c) as well as for separation into c-TiN and stable h-AlN (indicated by c–h) are added. Furthermore, the influence of strain and surface energy on the locus of the spinodal for the decomposition of c-$Ti_{1-x}Al_xN$ is presented as described in Ref. [13], and compared to the chemical spinodal. The phase diagram is limited in temperature by the melting of the nitride phases and/or their dissociation into metal and nitrogen. The eutectic concentration and temperature in the quasi-binary system TiN□ AlN was reported to be approximately at $x = 0.40$ and 2500 °C [20], while TiN and AlN melt (dissociate) at approximately 3290 and 2800 °C [21], respectively. These data are indicated in Fig. 3 by dotted lines.

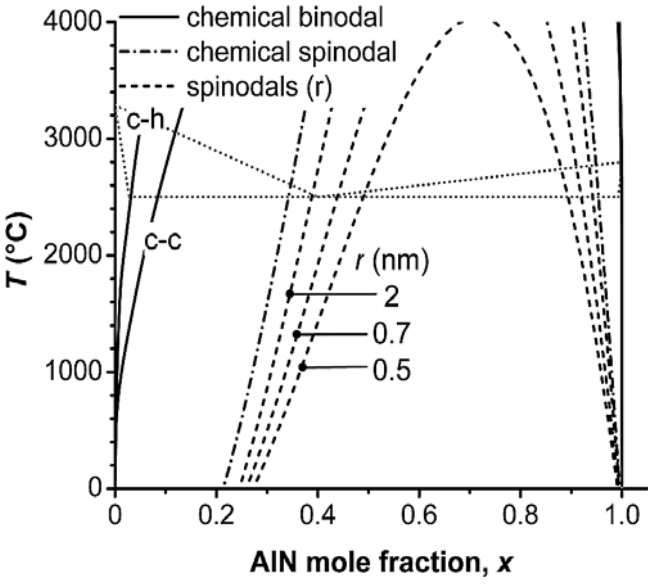

Fig. 3. Calculated temperature–composition phase diagram for c-$Ti_{1-x}Al_xN$ showing the influence of different particle radii r and strain energy on the spinodal, spinodals (r). The chemical binodals (solid lines) for decomposition into c-TiN and c-AlN (c–c) and into c-TiN and h-AlN (c–h) are added. The quasibinary system is indicated by dotted lines.

In the following, decomposition of c-$Ti_{1-x}Al_xN$ into its corresponding binary cubic phases (concentrations at the binodal) is discussed for $T = 1100$ °C and the spinodal decomposition is discussed for $T = 900$ °C. These temperatures are chosen based on our DSC and XRD investigations, showing that after annealing at ~1100 °C cubic phases of different lattice parameter and composition are formed, see Fig. 2b and Ref. [4]. After annealing at ~900 °C almost no difference between the formed phases and the matrix is detectable, see Ref. [4], thus these will be referred to as domains (TiN or AlN rich).

As during decomposition, the cubic domains are coherent among themselves and with the matrix, and the lattice initially remains continuous, elastic strain in the individual domains and matrix will build up. To a first approximation, this is based on continuous changes of the elastic constants as well as lattice parameters with the chemical composition of cubic $Ti_{1-x}Al_xN$ [11]. In a recent paper [13] we showed that this strain energy, calculated by continuum mechanical approaches (both modulus and lattice parameter misfit between the matrix and the two decomposition products, which are assumed to be spherical particles based on SANS measurements, are considered), is ~2.72, 2.99, and 2.12 kJ mol^{-1} with $x = 0.66$, 0.50, and 0.25 in case of a complete decomposition into c-TiN and c-AlN.

The energy related to the formation of new interfaces ($E_{surface}$) is also presented in Ref. [13] and can be calculated after:

$$E_{surface} = \frac{3\gamma}{r}$$

assuming the formation of spherical domains with radii r and specific surface energy γ. The specific surface energy for the decomposition into c-TiN and c-AlN is 0.182, 0.170, and 0.090 J m^{-2} for $x = 0.66$, 0.50 and 0.25, respectively. For comparison, the energy of symmetrical twin boundaries in intermetallic TiAl alloys is 0.076 J m^{-2} [22]. Details of the calculation of the surface energy using the broken bond hypothesis can be found in Ref. [13].

In order to detect the size of the domains and phases formed during annealing of cubic $Ti_{1-x}Al_xN$ coatings, for calculating $E_{surface}$, small-angle neutron scattering is performed on c-$Ti_{0.5}Al_{0.5}N$ in the as-deposited state and after heating to 860 and 1100 °C and subsequent cooling to RT, see Fig. 4a. Figure 4b shows their baseline subtracted scattering curves, where the as-deposited c-$Ti_{0.5}Al_{0.5}N$ measurement was used as the baseline. With increasing the maximum heating temperature from 860 to 1100 °C the interference maximum shifts from 2.5 nm^{-1} to a smaller q value of approximately 0.5 nm^{-1}, which indicates domain growth. Defining a characteristic size as $l_c = \pi/q_{max}$ thus gives a growth from 1.3 to 6.0 nm. Unfortunately, the accessible q-region was limited at small q so that a distinct maximum is not observed for the sample heated to 1100 °C. A dash-dotted line with the slope of q^{-4} is added to the plot to show which part of the scattering curve (1100 °C) is proportional to q^{-4}. However, a Guinier analysis [23] of the scattering curve gives a Guinier-radius of 3.2 nm, confirming the characteristic sizes. Finally, the scattering curves are also analyzed in terms of a Gaussian

size distribution of spherical particles in the framework of a two-phase model [24], giving the dashed lines in Fig. 4b. While this is assumed to be a good approximation for the sample heated to 1100 °C, where decomposition is in a later stage such that particles with a sharp compositional modulation have developed, it is expected to be only a rough approximation for the sample heated to 860 °C where spinodal decomposition should still be active. For the description of the maximum in the cross-section of the latter sample, interparticle interference was additionally taken into account by applying the local monodisperse approximation described by Pedersen [25]. For the latter, the Percus–Yevick approximation [26] is used to calculate the structure factor of the monodisperse hard-sphere model. The difference in scattering length density between particle and matrix has to be known for obtaining a correct particle volume fraction that controls the interference effect. Since this information cannot be provided yet, it is estimated such that a reasonable interference function is obtained. The size distributions resulting from the fits have mean radii of 0.7 and 2.9 nm (diameter of 1.4 and 5.8 nm), which are in good agreement with the above numbers. Thus, it is concluded that the SANS data indicate a domain size of ~1.4 nm for the sample heated to 860 °C and a mean particle size (diameter) of ~5.8 nm for the sample heated to 1100 °C.

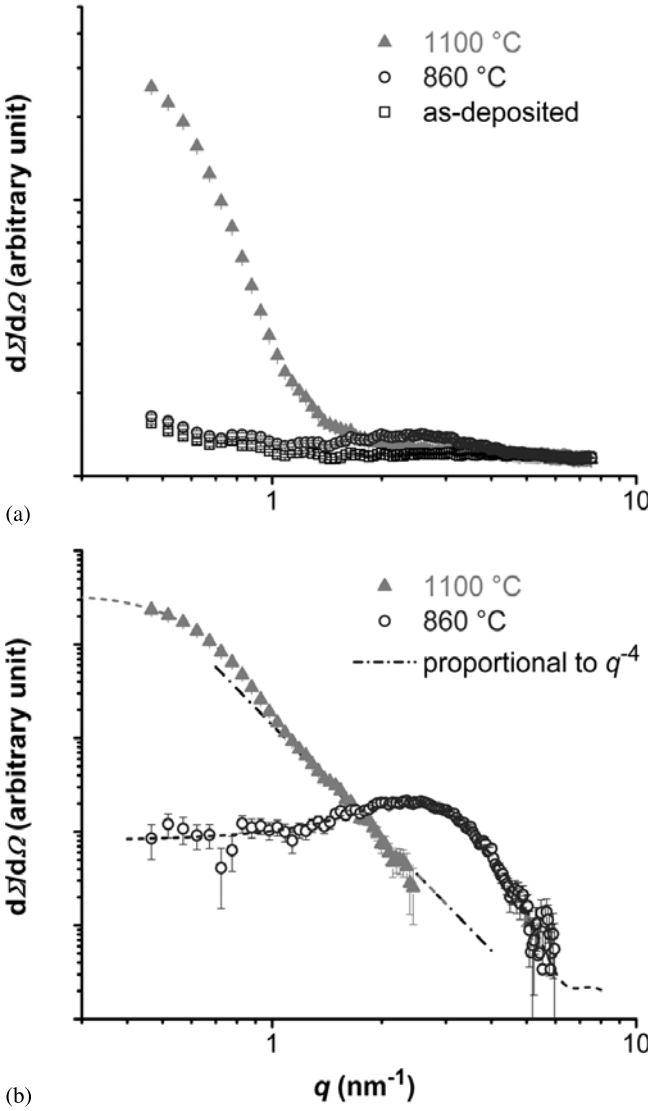

Fig. 4. (a) SANS scattering curves of c-$Ti_{0.5}Al_{0.5}N$ in the as-deposited state and after heating to 860 and 1100 °C and subsequent cooling to RT. The curves are shifted such that the high-q-tails fall together. (b) Baseline subtracted SANS curves with indicated q^{-4} slope for the 1100 °C curve (dash-dotted line). The dashed lines show the performed fit to determine the domain radii (see text).

Based on the data obtained by ab-initio calculation and continuum mechanics we can describe possible processes operating during annealing of supersaturated cubic $Ti_{1-x}Al_xN$ using DSC spectra, XRD analyses, and SANS data as presented in Figs. 1, 2, and 4, respectively.

Table 1 lists a comparison of the enthalpy outputs obtained by DSC and the different modeled energy contributions for $Ti_{1-x}Al_xN$ coatings with $x = 0$, 0.25, 0.50, and 0.66 for decomposition into separate metastable cubic phases. Including the strain and surface energy related to particles with ~2.9 nm radius at $T = 1100$ °C the c–c binodal includes compositions in the range of $x = 0.03-1$. The difference in energy of formation between cubic $Ti_{1-x}Al_xN$ and the underlying cubic phases (c-$Ti_{0.97}Al_{0.03}N$ and c-AlN) is 27.26, 25.67, and 13.27 kJ mol^{-1} for $x = 0.66$, 0.50 and 0.25, respectively. With these values the corresponding surface energies for particles with ~2.9 nm in radius are calculated to be 1.99, 1.88, and 0.97 kJ mol^{-1} for $x = 0.66$, 0.50 and 0.25 after Ref. [13]. Strain energies are reduced from the values obtained by continuum mechanics, which are based on a separation into phases with $x = 0$ and 1, to 2.65, 2.89, and 1.98 kJ mol^{-1} for $x = 0.66$, 0.50, and 0.25. Consequently, the theoretically available energy difference (ΔE, including strain and surface energy for a particle radius of 2.9 nm) for the decomposition of cubic $Ti_{1-x}Al_xN$ into c-$Ti_{0.97}Al_{0.03}N$ and c-AlN (binodal points at $T \sim 1100$ °C) is 22.62, 20.90, and 10.32 kJ mol^{-1} for $x = 0.66$, 0.50, and 0.25, respectively. The enthalpy output during DSC, subtracting the above mentioned contribution of recrystallization and c ? h transformation of AlN, is 20.49, 17.98, and 7.46 kJ mol^{-1} for $x = 0.66$, 0.50, and 0.25, which corresponds to the calculated values.

Annealing of c-TiN and h-AlN up to ~900 °C results in an energy release of 0.80 and 0.78 kJ mol^{-1} due to reduction of their defects content [4]. Similar values are expected for recovery processes active in c-$Ti_{1-x}Al_xN$ which have to be subtracted from the above mentioned experimental

Table 1. Comparison between measured enthalpy output ΔH_{DSC} during DSC up to 1400 °C (after subtracting the contribution of recrystallization and c ? h transformation of AlN) and the calculated energy difference ΔE for decomposition of c-$Ti_{1-x}Al_xN$ into phases at the binodal ($x = 0.03$ and 1 at $T = 1100$ °C, see Fig. 3), obtained from the energy of formation difference ΔE_f, the strain energy E_{strain}, and surface energy $E_{surface}$ for particle sizes of 2.9 nm in radius ($\Delta E = \Delta E_f - E_{strain} - E_{surface}$). All enthalpies and energies are stated in kJ mol^{-1}.

AlN mole fraction, x	Experiment	Modeling			
	ΔH_{DSC}	ΔE_f	E_{strain}	$E_{surface}$	ΔE
0.66	20.49	27.26	2.65	1.99	22.62
0.50	17.98	25.67	2.89	1.88	20.90
0.25	7.46	13.27	1.98	0.97	10.32
0	0.80	–	–	–	–

enthalpy outputs for the comparison with the calculations (see Table 1). Considering this influence of ~ 0.80 kJ mol^{-1} the deviation between enthalpy output during DSC and ΔE for the decomposition of cubic $Ti_{1-x}Al_xN$ into c-$Ti_{0.97}Al_{0.03}N$ and c-AlN is ~ 6, 10, and 20 % of ΔE, for $x = 0.66$, 0.50, and 0.25, respectively.

The modeled spinodal contribution to the decomposition of our $Ti_{1-x}Al_xN$ coatings with $x = 0.25$, 0.50, and 0.66 is based on the separation into domains at the spinodal with $T = 900\,^{\circ}$C. Phases within the spinodal region will decompose by the spinodal mechanism into phases at the spinodal, whereas further decomposition into phases outside the spinodal requires nucleation and growth. For the latter type of transformation, there is an associated activation energy barrier which effectively hinders the process which is in agreement with our observations of no precipitation, at our annealing conditions [4]. Including the strain and surface energy for a domain radius of 0.7 nm at $T = 900\,^{\circ}$C the spinodal includes composition in the range of $x = 0.33-0.97$, see Fig. 3. The difference in energy of formation between cubic $Ti_{1-x}Al_xN$ and the underlying cubic domains at the spinodal (c-$Ti_{0.67}Al_{0.33}N$ and c-$Ti_{0.03}Al_{0.97}N$) is 16.14 and 11.20 kJ mol^{-1} for $x = 0.66$ and 0.50. For temperatures above $\sim 640\,^{\circ}$C the alloy with $x = 0.25$ is outside the chemical spinodal, see Fig. 3. Based on these data the surface energy related to 0.7 nm radii domains is 4.89 and 3.40 kJ mol^{-1} and the strain energy is 1.35 and 1.01 kJ mol^{-1} for $x = 0.66$ and 0.50, respectively, calculated after Ref. [13]. Consequently, the modeled available energy difference ΔE (including strain and surface energy for a particle radius of 0.7 nm) for the spinodal decomposition of cubic $Ti_{1-x}Al_xN$ into c-$Ti_{0.67}Al_{0.33}N$ and c-$Ti_{0.03}Al_{0.97}N$ (spinodal points at $T \sim 900\,^{\circ}$C) is 9.81 and 6.79 kJ mol^{-1} for $x = 0.66$ and 0.50, respectively. These data and the temperature T_a up to which the integrated area under the corresponding DSC curves (reduced by the above mentioned contribution for recovery of ~ 0.80 kJ mol^{-1}) equals ΔE are presented in Table 2. The comparison between modeling and DSC data indicates that the decomposition of our $Ti_{1-x}Al_xN$ coatings is based on the spinodal mechanism up to 900 and 830 °C for $x = 0.66$ and 0.50, respectively. At higher temperatures the decomposition is also driven by nucleation and growth of phases with chemical compositions at the binodal. For the film with $x = 0.25$ the enthalpy output during DSC investigation equals that for recovery effects of TiN (0.80 kJ mol^{-1}) up to 670 °C. This temperature is already outside the chemical spinodal for $x = 0.25$. Consequently, in this case spinodal decomposition is unlikely.

It has to be mentioned that deviations between modeling and experiment can also be due to the degree of transformation during the experiment. In the model presented here a complete transformation is assumed. Also, the description of a random alloy influences the transformation energetics [27]. The thereby obtained energy of formation deviates by £2 % from the values calculated using a supercell approach, where the positions for Ti and Al ions at the metal sublattice are randomly chosen [11]. There, we have shown that the Al distribution and hence the number of Ti–Al bonds in $Ti_{1-x}Al_xN$ induce changes of the electronic structure, bond energy, and configurational entropy. Hence, the Al distribution has a strong influence on the energy of formation [11]. Although, these contributions are included in the calculations used here, they indicate that structural defects (i.e., point, line, and area defects) present in conventionally grown films have their impact on the energies as well. Furthermore, the calculation of spinodal and binodal is obtained using the approximation of a regular solution for the configurational entropy and is therefore associated with the well-known limitations of the regular solution model. However, the influence of internal strain and surface energy on the Gibbs free energy and hence on the temperature and composition range of the spinodal, as shown in Fig. 3, will be conserved if a more accurate description of the temperature dependent entropy term is employed. As for decomposition thermal activation is needed and the spinodal points come closer with increasing temperature the difference between matrix and spinodally separated domains becomes smaller, making experimental investigations by high-resolution transmission electron microscopy and XRD challenging. The $Ti_{1-x}Al_xN$ coating with $x = 0.66$ studied here, representing the most valued alloy coatings with compositions around 0.67, is deepest within the spinodal and offers the highest spinodal contribution to the decomposition process (see Table 2).

Table 2. Temperature T_a up to which the measured enthalpy output detected during DSC (after subtracting the contribution of recovery effects of 0.80 kJ mol^{-1}, see Table 1 for $x = 0$) equals the calculated energy difference ΔE for decomposition of c-$Ti_{1-x}Al_xN$ into domains with chemical compositions at the spinodal ($x = 0.33$ and 0.97 at $T = 900\,^{\circ}$C, see Fig. 3). The latter is obtained from the energy of formation difference ΔE_f, the strain energy E_{strain}, and surface energy $E_{surface}$ for a particle size of 0.7 nm in radius ($\Delta E = \Delta E_f - E_{strain} - E_{surface}$). All enthalpies and energies are stated in kJ mol^{-1}.

AlN mole fraction, x	Experiment	Modeling			
	T_a(°C)	ΔE_f	E_{strain}	$E_{surface}$	ΔE
0.66	900	16.14	1.35	4.98	9.81
0.50	830	11.20	1.01	3.40	6.79
0.25	670	–	–	–	–

4. Conclusions

Based on structural investigations by X-ray diffraction and small-angle neutron scattering and a comparison between experimentally obtained enthalpy output during differential scanning calorimetry with calculated energy differences using a combination of ab-initio calculations and continuum mechanics we can conclude that spinodal decomposition is present in c-$Ti_{1-x}Al_xN$ coatings with $x = 0.50$ and 0.66, whereas the alloy with $x = 0.25$ is outside the spinodal. Strain energy due to the formation of domains with different lattice parameter and elastic constants as well as surface energy related to the formation of new interfaces reduce the temperature and composition range of the chemical spinodal. Thus, in addition to coherency strain influence, the matrix and formed domains come closer in lattice parameter. These results and the fact that the formed domains are usually small explain the difficulties in observing spinodal decomposition for this type of materials.

The authors are thankful to J. Sjölén and L. Karlsson (SECO Tools AB) for providing the coating samples and H. Eckerlebe (GKSS) for carrying out the SANS measurements. P.H.M. acknowledges financial support by the Erwin Schrödinger Program (project J2469-N02) of the Austrian Science Fund (FWF). L.H. is supported from the Swedish Research Council (VR) and the Swedish Strategic Research Foundation (SSF). J.M.S. gratefully acknowledges funding from DFG (Schn 735/9-1).

References

[1] W.D. Münz: J. Vac. Sci. Technol. A 4 (1986) 2717.
[2] O. Knotek, M. Böhmer, T. Leyendecker: J. Vac. Sci. Technol. A 4 (1986) 2695.
[3] S.-D. Kim, I.-S. Hwang, J.-K. Rhee, T.-H. Cha, H.-D. Kim: Electrochem. Solid-State Lett. 4 (2001) G7.
[4] P.H. Mayrhofer, A. Hörling, L. Karlsson, J. Sjölén, T. Larsson, C. Mitterer, L. Hultman: Appl. Phys. Lett. 83 (2003) 2049.
[5] S. Veprek, H.-D. Männling, M. Jilek, P. Holubar: Mat. Sci. Eng. A 366 (2004) 202.
[6] R.F. Zhang, S. Veprek: Mat. Sci. Eng. A 448 (2007) 111.
[7] J.D. van der Waals: Z. Phys. Chem. 5 (1890) 133.
[8] J.W. Gibbs: The scientific papers of J.W. Gibbs, Vol. 1. Thermodynamics, Dover Publications, New York (1961) 105.
[9] T.W. Barbee, W.H. Holmes, D.L. Keith, M.K. Pyzyna, G. Ilonca: Thin Solid Films 45 (1977) 591.
[10] J.W. Cahn: Trans. Met. Soc. AIME 242 (1968) 166.
[11] P.H. Mayrhofer, D. Music, J.M. Schneider: J. Appl. Phys. 100 (2006) 094906.
[12] P.H. Mayrhofer, D. Music, J.M. Schneider: Appl. Phys. Lett. 88 (2006) 071922.
[13] P.H. Mayrhofer, F.D. Fischer, H. Böhm, C. Mitterer, J. M. Schneider: Acta Mater. 55 (2007) 1441.
[14] L. Karlsson: PhD thesis, (Linköping Studies in Science and Technology, dissertation no. 565, Linköping University, Sweden 1999).
[15] A. Hörling, L. Hultman, M. Odén, J. Sjölén, L. Karlsson: Surf. Coat. Technol. 191 (2005) 384.
[16] G. Kresse, J. Hafner: Phys. Rev. B 48 (1993) 13115.
[17] G. Kresse, J. Joubert: Phys. Rev. B 59 (1999) 1758.
[18] P.H. Mayrhofer, C. Mitterer, L. Hultman, H. Clemens: Prog. Mater. Sci. 51 (2006) 1032.
[19] F.J. Humphreys, M. Hatherly: Recrystallization and Related Annealing Phenomena, Pergamon, Oxford (1995).
[20] H. Holleck: Surf. Coat. Technol. 36 (1988) 151.
[21] T.B. Massalski: Binary Alloy Phase Diagrams, ASM International, Metals Park, OH (1990).
[22] L.E. Murr: Interfacial Phenomena in Metals and Alloys, Addison-Wesley, Reading, MA (1975).
[23] A. Guinier, G. Fournet: Small-Angle Scattering of X-Rays, John Wiley&Sons, New York (1955).
[24] G. Kostorz, in: G. Kostorz, H. Herman (Eds.), Treatise on Materials Science and Technology, Vol. 15: Neutron Scattering, Academic Press, New York (1979) 226.
[25] J.S. Pedersen: J. Appl. Cryst. 27 (1994) 595.
[26] D.J. Kinning, E.L. Thomas: Macromolecules 17 (1984) 1712.
[27] B. Alling, A.V. Ruban, A. Karimi, O.E. Peil, S.I. Simak, L. Hultman, I.A. Abrikosov: Phys. Rev. B 75 (2007) 045123.

(Received March 16, 2007; accepted August 2, 2007)

Bibliography

DOI 10.3139/146.101570
Int. J. Mat. Res. (formerly Z. Metallkd.)
98 (2007) 11; page 1054–1059
Carl Hanser Verlag GmbH & Co. KG
ISSN 1862-5282

Correspondence address

Dr. Paul H. Mayrhofer
Department of Physical Metallurgy and Materials Testing
Montanuniversität Leoben
Franz Josef Straße 18, A-8700 Leoben, Austria
Tel.: +43 3842 402 4211
Fax: +43 3842 402 4202
E-mail: mayrhofer@mu-leoben.at